Pergamon

Int. J. Solids Structures Vol. 33, No. 8, pp. 1157–1174, 1996

0020–7683/96 $15.00 + .00

0020–7683(95)00069–0

ULTRASONIC STRESS MEASUREMENTS BASED ON THE GENERALIZED ACOUSTIC RATIO TECHNIQUE

HANS R. DORFI and HENRY R. BUSBY†
Department of Mechanical Engineering, The Ohio State University, Columbus, OH 43210, U.S.A.

and

MICHAEL JANSSEN

Department of Materials Science, Delft University of Technology, Delft, The Netherlands

(*Received* 20 *July* 1994; *in revised form* 17 *March* 1995)

Abstract—Based on the theory of wave propagation in prestressed solids, a new stress reconstruction method, the Generalized Acoustic Ratio (GAR) technique, is developed for locally plane geometries. The GAR method requires the measurement of the time of flight of the three ultrasonic wave modes (longitudinal and shear waves) perpendicular to the plane of stress and the associated shear wave polarization angles. From this ultrasonic data and calibrated material properties, the local plane stress tensor is determined. Measurements on uniaxial tension test specimens yield the acoustoelastic calibration constants.

INTRODUCTION

The nondestructive measurement of applied and residual stresses is an area of great interest to engineers. Compared to diffraction methods, which are commonly used for nondestructive stress measurements, ultrasonic techniques are both less expensive and faster. Therefore, they hold great promise as practical nondestructive methods for stress measurement.

Because of its analogy to photoelasticity, the area of ultrasonic stress measurements in solids is termed acoustoelasticity. The theory of acoustoelasticity originated from the interest in the measurement of third-order elastic constants (TOECs) in crystals. These elastic constants are needed to account for the small nonlinear elastic effects in hyperelastic solids. Hughes and Kelly (1953) developed the theory of acoustoelasticity and used ultrasonic waves to determine these constants in crystals by varying the applied stress. Toupin and Bernstein (1961) extended their work to hyperelastic materials with arbitrary symmetry. Benson and Raelson (1959) and Bergman and Shahbender (1958) were the first engineers to employ ultrasonic waves for stress measurements in solids.

Based on the early theoretical work, Thurston and Brugger (1964) refined the theory and introduced the natural velocity, which refers to the undeformed (natural) state. The natural velocity is not the real wave velocity; since only the time of flight is measured directly, the velocity is found by reference to the ultrasonic path length. One may either choose the actual path length or the one prior to deformation. In measurements it is frequently useful to refer to the original undeformed path length, since it is independent of the applied load.

Most acoustoelastic theories are based on the assumption that the body is in a hyperelastic state of stress; while this assumption is satisfied frequently, it is not valid for stress induced by local plastic deformation because of the localized change in material parameters. Therefore, the identification of residual stresses caused by plastic deformation has been less reliable (Crecraft, 1967). Furthermore, most materials exhibit slight anisotropy or texture due to the fabrication process. The change in wave speed is not only affected by stresses

† To whom correspondence should be addressed.

but also by this anisotropy. Since both stress- and texture-induced velocity shifts are usually of similar magnitude, it has been difficult to separate them.

Despite these difficulties, acoustoelastic techniques are becoming more popular. New ultrasonic transducers have improved the accuracy of the measurements. This is particularly important since the acoustoelastic effect is rather small; typically, the relative change in wave speed is of the order of 0.001% per MPa of applied stress in aluminum. Competing effects intrinsic to the specimen are elastic anisotropy and material inhomogeneity. Acoustoelastic methods are therefore essentially limited to material regions, which are reasonably uniform both in microstructure and composition.

To overcome the problems of earlier techniques, the Generalized Acoustic Ratio (GAR) method is proposed. It is based on the simultaneous measurement of the time of flight of the three ultrasonic wave modes (longitudinal and shear waves) perpendicular to the plane of stress and the associated shear wave polarization angles. The GAR technique has several advantages: since it is based on wave speed ratios and the waves travel along an identical ultrasonic flight path, no length measurement is necessary; also, the transit time measurement errors due to temperature fluctuations result in small errors in the stress predictions. Furthermore, the absolute local stress is predicted at each measurement point.

ACOUSTOELASTIC THEORY

The propagation of plane ultrasonic waves in a stressed elastic medium is governed by the acoustoelastic theory. To simplify the theoretical analysis it is generally assumed that the deformation and stress states are locally homogeneous.

To develop the acoustoelastic equations it is assumed that the body of interest undergoes three different states: in the natural state the body is free of stress and strain (undeformed configuration). After load application the body changes to its initial state, a static state with residual or applied stress. Depending on the loading history the body may have experienced elastic or plastic deformation. To identify the stresses an ultrasonic wave motion is superposed. Thus, the body is further deformed to its final state. The deformation from the initial to the final state is assumed to be small and elastic. This assumption is certainly valid for low power ultrasonic wave motion. However, the deformation from the natural to the initial state may be large.

It is possible to develop the acoustoelastic equations either with respect to the natural state or the initial state. Equations derived with respect to the natural state are particularly useful for the analysis of hyperelastic materials under varying load conditions. This approach will be followed here.

The nomenclature most commonly used in the literature is adopted (Pao *et al.*, 1984). To distinguish the different states we use Greek letters and indices for quantities referring to the natural state (position vector ξ, components ξ_α), capital letters for reference to the initial state ($\mathbf{X}, X_A$) and lower case for the final state ($\mathbf{x}, x_a$). Physical quantities are also denoted by superscripts 0, i, f for the respective states. Figure 1 shows the body and a typical point P in its three states.

Displacements and strains

The displacements from the natural to the initial and final states are given by

$$\mathbf{u}^{\mathrm{i}}(\xi) = \mathbf{X} - \xi \quad \mathbf{u}^{\mathrm{f}}(\xi, t) = \mathbf{x} - \xi \tag{1}$$

and the incremental displacement from the initial to the final state is given by

$$\mathbf{u}(\xi, t) = \mathbf{x} - \mathbf{X} = \mathbf{u}^{\mathrm{f}} - \mathbf{u}^{\mathrm{i}}. \tag{2}$$

Note that the initial deformation $\mathbf{u}^{\mathrm{i}}$ is static. In the following derivation the equations will be given in the convenient index notation; summation over repeated indices is implied

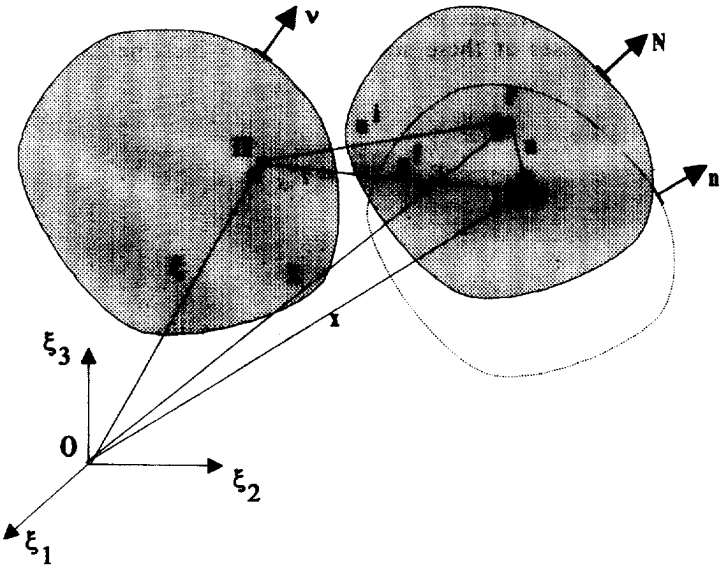

Fig. 1. Body in its natural (x), initial (X) and final states (x).

unless otherwise noted. We define two different deformation gradients, deformation of initial with respect to natural state and final to natural state:

$$F^{\mathrm{i}}_{\mathrm{I}\alpha} = \frac{\partial X_{\mathrm{I}}}{\partial \xi_\alpha} \quad F^{\mathrm{f}}_{\mathrm{i}\alpha} = \frac{\partial x_{\mathrm{i}}}{\partial \xi_\alpha}. \tag{3}$$

As strain measure the Lagrangian strain tensor is adopted. Again, there are two different strain measures in analogy to the two different deformation gradients, the Lagrangian strain in the initial state referred to the natural configuration and the Lagrangian strain in the final state referred to the natural configuration:

$$E^{\mathrm{i}}_{\alpha\beta} = \frac{1}{2}\left(\frac{\partial u^{\mathrm{i}}_\alpha}{\partial \xi_\beta} + \frac{\partial u^{\mathrm{i}}_\beta}{\partial \xi_\alpha} + \frac{\partial u^{\mathrm{i}}_\gamma}{\partial \xi_\beta}\frac{\partial u^{\mathrm{i}}_\gamma}{\partial \xi_\alpha}\right) \tag{4}$$

$$E^{\mathrm{f}}_{\alpha\beta} = \frac{1}{2}\left(\frac{\partial u^{\mathrm{f}}_\alpha}{\partial \xi_\beta} + \frac{\partial u^{\mathrm{f}}_\beta}{\partial \xi_\alpha} + \frac{\partial u^{\mathrm{f}}_\nu}{\partial \xi_\beta}\frac{\partial u^{\mathrm{f}}_\nu}{\partial \xi_\alpha}\right). \tag{5}$$

The difference of the initial strain to final strain with respect to the natural state is given in terms of the displacement gradients as

$$E_{\alpha\beta} = \frac{1}{2}\left(\frac{\partial u_\alpha}{\partial \xi_\beta} + \frac{\partial u_\beta}{\partial \xi_\alpha} + \frac{\partial u^{\mathrm{i}}_\nu}{\partial \xi_\alpha}\frac{\partial u_\nu}{\partial \xi_\beta} + \frac{\partial u^{\mathrm{i}}_\nu}{\partial \xi_\beta}\frac{\partial u_\nu}{\partial \xi_\alpha}\right), \tag{6}$$

where terms quadratic in the incremental displacement gradient are neglected.

Stresses

In nonlinear continuum mechanics, several stress tensors are used: the Cauchy stress in the deformed configuration (**t**), the first Piola–Kirchhoff (P–K) stress (**P**), which relates the force in the deformed configuration to the surface element prior to deformation, and the second P–K stress (**T**), which is defined on the undeformed surface area and is related to the first P–K stress by a transformation of the stress by the deformation gradient.

We define the incremental second P–K stresses from the initial to the final state as the difference of the stresses at these states (note that incremental quantities are not superscripted):

$$T_{\alpha\beta} = T^{\mathrm{f}}_{\alpha\beta} - T^{\mathrm{i}}_{\alpha\beta}. \tag{7}$$

Equation of motion

To relate the ultrasonic wave motion to the predeformation, an incremental equation of motion has to be derived. It is assumed that the predeformation is static and body forces are neglected; therefore, its stress field is governed by the equilibrium equation, which is expressed in terms of the second P–K stress and the displacement gradient as

$$\frac{\partial}{\partial \xi_\alpha}\left(T^{\mathrm{i}}_{\alpha\gamma}\left(\delta_{\beta\gamma} + \frac{\partial u^{\mathrm{i}}_\beta}{\partial \xi_\gamma}\right)\right) = 0. \tag{8}$$

The equation of motion in the final state is given by

$$\frac{\partial}{\partial \xi_\alpha}\left(T^{\mathrm{f}}_{\alpha\gamma}\left(\delta_{\beta\gamma} + \frac{\partial u^{\mathrm{f}}_\beta}{\partial \xi_\gamma}\right)\right) = \rho^0 \frac{\partial^2 u^{\mathrm{f}}_\beta}{\partial t^2}. \tag{9}$$

To obtain an incremental equation of motion we subtract eqn (8) from eqn (9). Substitution of the incremental stress (7) and displacement (2) yields

$$\frac{\partial}{\partial \xi_\alpha}\left(T_{\alpha\beta} + T^{\mathrm{i}}_{\alpha\gamma}\frac{\partial u_\beta}{\partial \xi_\gamma} + T_{\alpha\gamma}\frac{\partial u^{\mathrm{i}}_\beta}{\partial \xi_\gamma}\right) = \rho^0 \frac{\partial^2 u_\beta}{\partial t^2}, \tag{10}$$

where products of incremental terms were neglected. It is important to note that the incremental equation is valid for any predeformation, large or small, elastic or plastic.

Constitutive law

In order to solve eqn (10), a constitutive law has to be postulated. Because of the small nonlinearities in the stress–strain relationship of polycrystalline materials, a hyperelastic constitutive law is frequently assumed. However, several other constitutive relations were proposed; they include effects of plastic deformation in order to account for the change in texture, which accompanies the plastic flow (Johnson, 1981; Pao *et al.*, 1991; Kobayashi, 1990). These theories require knowledge of the plastic deformation history and are thus very limited in their applicability.

In this work a hyperelastic predeformation is assumed. Thus, all incremental quantities can be referred to the undeformed state. The non-linear stress–strain relationship is given by (Pao *et al.*, 1984)

$$T^{\mathrm{i,f}}_{\alpha\beta} = C^0_{\alpha\beta\gamma\delta}E^{\mathrm{i,f}}_{\gamma\delta} + \tfrac{1}{2}C^0_{\alpha\beta\gamma\delta\varepsilon\eta}E^{\mathrm{i,f}}_{\gamma\delta}E^{\mathrm{i,f}}_{\varepsilon\eta}, \tag{11}$$

where $C^0_{\alpha\beta\gamma\delta}$ and $C^0_{\alpha\beta\gamma\delta\varepsilon\eta}$ denote the second and third order elastic constants in the undeformed state and the superscript denotes quantities at the initial or final state. For a purely hyperelastic formation, the constitutive law can be expanded into a power series about the initial state as

$$T^{\mathrm{f}}_{\alpha\beta} = T^{\mathrm{i}}_{\alpha\beta} + \left.\frac{\partial T^{\mathrm{f}}_{\alpha\beta}}{\partial E^{\mathrm{f}}_{\gamma\delta}}\right|_{E=E^{\mathrm{i}}} (E^{\mathrm{f}}_{\gamma\delta} - E^{\mathrm{i}}_{\gamma\delta}) + \cdots \tag{12}$$

With the definitions of the incremental strains and stresses in eqns (6) and (7) and the hyperelastic constitutive law (11), the incremental constitutive law is found as

$$T_{\alpha\beta} = (C^0_{\alpha\beta\gamma\delta} + C^0_{\alpha\beta\gamma\delta\varepsilon\eta} E^{\mathrm{i}}_{\varepsilon\eta}) E_{\gamma\delta}. \tag{13}$$

Substitution of eqn (13) into the incremental equation of motion yields

$$\frac{\partial}{\partial \xi_\beta}\left(T^{\mathrm{i}}_{\beta\gamma}\frac{\partial u_\alpha}{\partial \xi_\gamma} + \Gamma_{\alpha\beta\gamma\delta}\frac{\partial u_\gamma}{\partial \xi_\delta}\right) = \rho^0 \frac{\partial^2 u_\alpha}{\partial t^2}, \tag{14}$$

where

$$\Gamma_{\alpha\beta\gamma\delta} = (C^0_{\sigma\beta\rho\delta} + C^0_{\sigma\beta\rho\delta\varepsilon\eta} E^{\mathrm{i}}_{\varepsilon\eta})\left(\delta_{\rho\gamma} + \frac{\partial u^{\mathrm{i}}_\nu}{\partial \xi_\rho}\delta_{\gamma\nu}\right)\left(\delta_{\alpha\sigma} + \frac{\partial u^{\mathrm{i}}_\alpha}{\partial \xi_\sigma}\right). \tag{15}$$

Note that $\Gamma_{\alpha\beta\gamma\delta}$ depends only on the initial deformation and the elastic constants in the natural state. For zero predeformation, $\Gamma_{\alpha\beta\gamma\delta}$ simplifies to $C^0_{\alpha\beta\gamma\delta}$.

The above expression can be simplified for small predeformation; retaining only terms linear in the displacement gradient, we get

$$\Gamma_{\alpha\beta\gamma\delta} = C^0_{\alpha\beta\gamma\delta} + C^0_{\alpha\beta\gamma\delta\varepsilon\eta}\frac{\partial u^{\mathrm{i}}_\varepsilon}{\partial \xi_\eta} + C^0_{\alpha\beta\rho\delta}\frac{\partial u^{\mathrm{i}}_\gamma}{\partial \xi_\rho} + C^0_{\rho\beta\gamma\delta}\frac{\partial u^{\mathrm{i}}_\alpha}{\partial \xi_\rho}. \tag{16}$$

For a homogeneous predeformation, eqn (14) simplifies to

$$A_{\alpha\beta\gamma\delta}\frac{\partial^2 u_\gamma}{\partial \xi_\beta \partial \xi_\delta} = \rho^0 \frac{\partial^2 u_\alpha}{\partial t^2}, \tag{17}$$

where $A_{\alpha\beta\gamma\delta} = (\Gamma_{\alpha\beta\gamma\delta} + T^{\mathrm{i}}_{\beta\delta}\delta_{\alpha\gamma})$ is constant for a given predeformation. Equation (17) is the incremental equation of motion of a hyperelastically and homogeneously predeformed medium.

Plane wave propagation

It is assumed that a plane sinusoidal wave propagates in the prestressed body, given by

$$u_\alpha = U_\alpha \mathrm{e}^{jk(n_\varepsilon \xi_\varepsilon - vt)} \tag{18}$$

where U is the particle displacement vector, n the direction of propagation, j the imaginary unit, v the propagation speed and k the wave vector. v is related to k by the relation $v = \omega/k$. Substitution into eqn (17) yields the Christoffel equations, a system of equations for the unknown displacement and its associated propagation speed.

$$(A_{\alpha\beta\gamma\delta} n_\beta n_\delta - \rho^0 v^2 \delta_{\alpha\gamma}) U_\gamma = 0. \tag{19}$$

For solutions to exist the determinant of the above system has to be zero. This is mathematically equivalent to finding the eigenvalues of $\rho^0 v^2$ of $D_{\alpha\gamma} = A_{\alpha\beta\gamma\delta} n_\beta n_\delta$. $D_{\alpha\gamma}$ is denoted as the acoustic tensor. Because of the symmetry of the stiffness coefficients the acoustic tensor

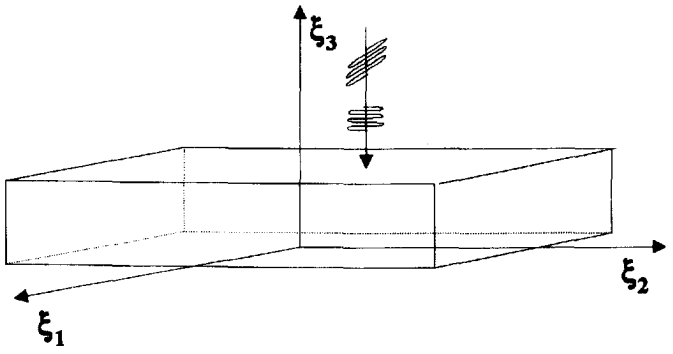

Fig. 2. Orthotropic body with acoustic wave propagation in the ξ_3 direction.

is symmetric and there exist three real values for the wave speeds and their associated eigenvectors; the displacement vectors are orthogonal to each other.

The Generalized Acoustic Ratio (GAR) technique

The GAR technique is based on the assumption that the body of interest can be modeled as a locally plane structure subjected to a two-dimensional stress field. The simple geometry allows the measurements of the time of flight of normal incidence waves reflected on the back face of the specimen. Also, the material symmetry is assumed to be orthotropic. The body and its reference frame are shown in Fig. 2. The orthotropic symmetry axes are parallel to the coordinate system and the acoustic waves propagate in the ξ_3 direction. In general, the principal stress axes do not coincide with the material axes; thus, the polarization axes of shear waves also differ from the material and stress axes (see Fig. 3).

For wave propagation in the ξ_3 direction ($n_\delta = \delta_{3\delta}$), the Christoffel equation (19) simplifies to

$$(A_{\alpha 3\gamma 3} - \rho^0 \delta_{\alpha\gamma} v^2) U_\gamma = 0. \tag{20}$$

To simplify the notation, the Voigt abbreviation is employed to contract the indices of the acoustic and elastic tensors. It is defined as the index mapping $11 \to 1$, $22 \to 2$, $33 \to 3$, $23 \to 4$, $13 \to 5$, $12 \to 6$. We assume that there is a one-to-one correspondence between the contracted elastic constants ($C^0_{\alpha\beta}$, $C^0_{\alpha\beta\gamma}$) and the elastic tensor ($C^0_{\alpha\beta\gamma\delta}$, $C^0_{\alpha\beta\gamma\delta\varepsilon\eta}$). Other researchers introduce factors to account for the multiplicity of constants (e.g. Hearmon, 1953).

The plane stress field $T^i_{\varepsilon\eta}$ is also conveniently written in contracted notation as $\{T^i_1, T^i_2, T^i_6\}$. Substitution of the stress field, the contracted orthotropic elastic constants and the acoustic tensor defined in eqns (16) and (17) into eqn (20) yields, after lengthy calculation,

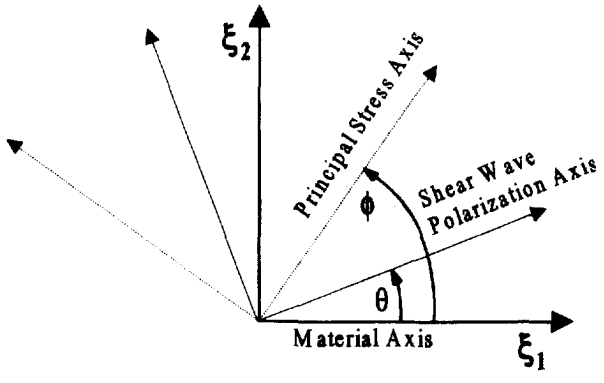

Fig. 3. Principal stress and acoustic axes in the ξ_1–ξ_2 plane.

$$\begin{bmatrix} C^0_{55}+s_{55}-\rho^0 v^2 & s_{45} & 0 \\ s_{45} & C^0_{44}+s_{44}-\rho^0 v^2 & 0 \\ 0 & 0 & C^0_{33}+s_{33}-\rho^0 v^2 \end{bmatrix} \mathbf{U} = 0, \tag{21}$$

where s_{ij} are the stress-induced terms given by

$$\begin{aligned} s_{jj} &= h_{j1} T^i_1 + h_{j2} T^i_2 \quad j = 3,4,5 \\ s_{45} &= h_{45} T^i_6 \end{aligned} \tag{22}$$

and h_{ij} depend only on the material properties in the undeformed state and are found as

$$\begin{aligned} h_{ij} &= \sum_{k=1}^{3} C^0_{kii} S^0_{jk} + 2C^0_{ii} S^0_{j(6-i)} \quad i = 3,4,5 \quad j = 1,2 \\ h_{45} &= (C^0_{44} + C^0_{55} + 2C^0_{456})(2S^0_{66}). \end{aligned} \tag{23}$$

The S^0_{ij} are the linear compliances, which can be expressed explicitly in terms of the linear elastic constants as

$$\begin{aligned} &S^0_{11} = (C^0_{22}C^0_{33} - C^{0^2}_{23})/d \quad S^0_{12} = S^0_{21} = (C^0_{13}C^0_{23} - C^0_{33}C^0_{12})/d \\ &S^0_{13} = (C^0_{12}C^0_{23} - C^0_{22}C^0_{13})/d \quad S^0_{23} = (C^0_{12}C^0_{13} - C^0_{11}C^0_{23})/d \\ &S^0_{66} = 1/(4C^0_{66}) \quad S^0_{22} = (C^0_{11}C^0_{33} - C^{0^2}_{13})/d \\ &d = C^0_{11}C^0_{22}C^0_{33} + 2C^0_{12}C^0_{13}C^0_{23} - C^0_{11}C^{0^2}_{23} - C^0_{22}C^{0^2}_{13} - C^0_{33}C^{0^2}_{12}. \end{aligned} \tag{24}$$

For nontrivial solution of eqn (21), its determinant has to be zero. This yields the three possible ultrasonic wave speeds v_{S1}, V_{S2}, V_L and their respective polarization vectors U (two pure shear waves and a pure longitudinal wave). Because of the off-diagonal zeroes, one solution is completely decoupled; its eigenvalue is easily recognized as

$$\rho^0 v_L^2 = C^0_{33} + h_{31} T^i_1 + h_{32} T^i_2, \tag{25}$$

with its associated eigenvector $\{0, 0, 1\}$, a pure longitudinal wave. The shear wave speeds are found from eqn (21) as

$$2\rho^0 v^2_{S1,S2} = C^0_{55} + C^0_{44} + s_{55} + s_{44} \pm [(C^0_{55} - C^0_{44} + s_{55} - s_{44})^2 + 4s^2_{45}]^{1/2}. \tag{26}$$

In experimental analysis it is preferable to use wave speed ratios. The GAR technique uses two of these ratios, the shear birefringence B and the inverse R-value IR:

$$B = 2\frac{v_{S1} - v_{S2}}{v_{S1} + v_{S2}} \quad IR = \frac{v_{S1} + v_{S2}}{2v_L}. \tag{27}$$

Measurement techniques based on the shear birefringence have been in use for many years. More recently, Toda *et al.* (1984) suggested the R-value, the ratio of the longitudinal wave speed to the average shear wave speed. Here we use the inverse R-value, which is simply the reciprocal of the above.

By taking the difference of the two shear wave speeds, the birefringence relation can be derived. Subtraction of v_{S1} from v_{S2} yields

$$\rho^0(v_{S1}^2 - v_{S2}^2) = [(C_{55}^0 - C_{44}^0 + s_{55} - s_{44})^2 + 4s_{45}^2]^{1/2}. \tag{28}$$

Together with $v_{10} = \sqrt{C_{55}^0/\rho^0}$ and $v_{20} = \sqrt{C_{44}^0/\rho^0}$ and the mean shear wave velocity $v_0 = (v_{S1} + v_{S2})/2 \approx (v_{10} + v_{20})/2$, the birefringence relation simplifies to

$$B = \frac{v_1 - v_2}{v_0} = \left[\left(B_0 + \frac{s_{55} - s_{44}}{2\rho v_0^2}\right)^2 + \left(\frac{s_{45}}{\rho v_0^2}\right)^2\right]^{1/2}, \tag{29}$$

where the initial birefringence B_0 is defined as $B_0 = (v_{10} - v_{20})/v_0$. Substitution of s_{ij} shows the stress dependence of the birefringence relation:

$$B = \left[\left(B_0 + \frac{(h_{51} - h_{41})T_1^i + (h_{52} - h_{42})T_2^i}{2\rho v_0^2}\right)^2 + \left(\frac{h_{45}T_6^i}{\rho v_0^2}\right)^2\right]^{1/2}. \tag{30}$$

Alternatively, the in-plane principal stresses S_1, S_2 and the principal stress angle ϕ can be used to define the stress state. Define the sum and difference of the principal stresses as $S_+^i = S_1^i + S_2^i$ and $S_-^i = S_1^i - S_2^i$. The prestress in the material coordinate system T_j^i is given in terms of the principal stresses as

$$T_{1,2}^i = \frac{S_+^i}{2} \pm \frac{S_-^i}{2}\cos 2\phi; \quad T_6^i = \frac{S_-^i}{2}\sin 2\phi. \tag{31}$$

Substitution of the principal stresses into the birefringence relation yields

$$B = [(B_0 + f_1 S_+^i + f_2 S_-^i \cos 2\phi)^2 + (f_3 S_-^i \sin 2\phi)^2]^{1/2}, \tag{32}$$

where the coefficients f_j are given by

$$f_1 = \frac{h_{51} + h_{52} - h_{41} - h_{42}}{4\rho v_0^2}; \quad f_2 = \frac{h_{51} - h_{52} - h_{41} + h_{42}}{4\rho v_0^2}; \quad f_3 = \frac{h_{45}}{2\rho v_0^2}. \tag{33}$$

The orthogonal polarization directions are given by $\{\cos\theta, \sin\theta, 0\}$ and $\{-\sin\theta, \cos\theta, 0\}$ and the angle θ is found from

$$\sin 2\theta = \frac{f_3 S_-^i}{B}\sin 2\phi; \quad \cos 2\theta = \frac{B_0 + f_1 S_+^i + f_2 S_-^i \cos 2\phi}{B}. \tag{34}$$

It is also possible to derive a second birefringence relation from the eigenvalue equation (26) by adding the two squared velocities. However, this relation requires absolute velocity measurements and is not of interest here.

The stress dependence of the longitudinal wave speed is found from eqn (25), which is rewritten as

$$v_3 = v_{30}[1 + s_L], \tag{35}$$

with $v_{30} = \sqrt{C_{33}^0/\rho^0}$ and

$$s_L = f_{31} S_+^i + f_{32} S_-^i \cos 2\phi, \tag{36}$$

where f_{ij} are defined by

$$f_{31} = \frac{h_{31}+h_{32}}{4C_{33}^0}; \quad f_{32} = \frac{h_{31}-h_{32}}{4C_{33}^0}. \tag{37}$$

Note that s_L is a small quantity, typically of the order of 1% or less.

For a strongly orthotropic material, the wave speed stress dependence of v_1 and v_2 is assumed to be linear and is found from a Taylor series expansion of eqn (26). To first order, the shear wave speed dependence is found as

$$v_{S1} = v_{10}(1+s_{S1}); \quad v_{S2} = v_{20}(1+s_{S2}), \tag{38}$$

where

$$s_{S1} = \frac{h_{51}T_1^i + h_{52}T_2^i}{2\rho^0 v_{10}^2} \quad s_{S2} = \frac{h_{41}T_1^i + h_{42}T_2^i}{2\rho^0 v_{20}^2}. \tag{39}$$

The inverse R-value IR is defined as the ratio of the average of the shear wave speeds to the longitudinal wave speed. With eqns (35) and (38), it is found as

$$IR = \frac{v_1+v_2}{2v_3} \approx IR_0\left(1+\frac{v_{10}(s_{S1}-s_L)+v_{20}(s_{S2}-s_L)}{v_{10}+v_{20}}\right), \tag{40}$$

where $IR_0 = (v_{10}+v_{20})/(2v_{30})$ is the initial inverse R-value in the stress-free state. Back-substitution of the stress dependence of s_{ij} yields the inverse R-value in terms of the stresses:

$$\Delta IR = \frac{IR-IR_0}{IR_0} = r_1 T_1^i + r_2 T_2^i = r_A S_+^i + r_B S_-^i \cos 2\phi, \tag{41}$$

with

$$r_j = \frac{1}{2}\left(\frac{h_{5j}}{2\rho^0 v_0 v_{10}} + \frac{h_{4j}}{2\rho^0 v_0 v_{20}} - \frac{h_{3j}}{C_{33}^0}\right); \quad r_A = \frac{r_1+r_2}{2}; \quad r_B = \frac{r_1-r_2}{2}. \tag{42}$$

Equations (32), (34) and (41) are four nonlinear equations in the unknowns S_+^i, S_-^i and ϕ to be solved for a given set of B, IR and θ and known material elastic constants. Recall that B and IR are ratios of time of flight measurements and θ is measured directly.

For the subsequent analysis we require that the birefringence is always positive. This can be ensured by simply subtracting the larger shear wave speed from the smaller one in the birefringence formula. The polarization angle is then defined as the angle between the polarization vector of the larger wave speed and the ξ_1 axis.

Even though the equations are nonlinear, they can be solved explicitly. Substitution of eqns (34) and (41) into the birefringence relation (32) and elimination of the terms $S_-^i \cos 2\phi$ and $S_-^i \sin 2\phi$ yields an expression for S_+^i only:

$$S_+^i = \left(-\Delta IR\frac{f_2}{r_B} + B\cos 2\theta - B_0\right)\left(\frac{r_B}{f_1 r_B - r_A f_2}\right). \tag{43}$$

Once S_+^i is calculated we can substitute the result into the birefringence equation (32) and solve for S_-^i. After some algebra and with the identity $\cos 2\theta = (1-\sin^2 2\theta)^{1/2}$, S_-^i is found as

$$S^i_- = \left[\left(\frac{r_A(B\cos 2\theta - B_0) - f_1 \Delta IR}{r_A f_2 - f_1 r_B}\right)^2 + \left(\frac{B\sin 2\theta}{f_3}\right)^2\right]^{1/2}. \tag{44}$$

The square root in the above equation implies that S^i_- may be either taken as positive or negative; we will choose S^i_- to be positive. In fact, it is immaterial which sign is chosen, because the principal stress angle ϕ is subsequently calculated from eqn (34). However, since $-\sin(2\theta) = \sin(2(\theta+90°))$, a change in the sign of S^i_- yields a principal stress angle $\phi+90°$, an interchange of principal stress axes.

For an isotropic material ($B_0 = f_1 = 0$, $f_3 = f_2$) the expression simplifies to the well known isotropic birefringence law:

$$S^i_- = \frac{B}{f_2}. \tag{45}$$

Once S^i_+ and S^i_- are calculated, the principal stress angle ϕ is calculated from eqn (34) as

$$\sin 2\phi = \frac{B}{f_3 S^i_-}\sin 2\theta \quad \cos 2\phi = \frac{B\cos 2\theta - B_0 - f_1 S^i_+}{f_2 S^i_-}. \tag{46}$$

It is of interest to determine the load states where the birefringence equals zero or, alternatively, where the two shear waves have identical wave speed. Substitution of $B = 0$ into eqn (44) and elimination of ΔIR yields the condition for zero birefringence:

$$B_0 + f_1 S^i_+ + f_2 S^i_- = 0. \tag{47}$$

From eqn (46), we conclude that the principal stress angle ϕ for zero birefringence has to be 0° or 90°. Note that for zero birefringence the polarization angle is indeterminate [eqn (34)], a "quasi-isotropic" state.

It is interesting to study the polarization angles in the neighborhood of acoustic "quasi-isotropy". For small angles ($\phi \ll 1$), eqn (34) can be approximated as

$$\tan 2\theta \approx \frac{f_3 S^i_- 2\phi}{B_0 + f_1 S^i + f_2 S^i_-}. \tag{48}$$

As the stress state approaches acoustic "quasi-isotropy" the denominator changes sign [eqn (47)] and the polarization angle rotates rapidly. This phenomenon is clearly observed in acoustoelastic experiments.

Equations (43), (44) and (46) form the GAR technique: for given acoustic ratios B, IR and polarization angle θ the local plane stress tensor is uniquely determined. The technique is valid for both isotropic and orthotropic materials and the material-dependent coefficients are typically found from calibration measurements.

The authors would like to point out that the GAR technique is an extension of the shear birefringence and the R-value technique. Both techniques do not yield sufficient information to determine the local stress state. Typically, additional information or the global stress field is used to determine the local stresses. By combining the two methods into one, the GAR technique can be derived, which yields the local plane stress tensor.

EXPERIMENTAL

The GAR technique is based on the assumption that the reference material is of orthotropic symmetry and deforms hyperelastically. To calibrate the acoustoelastic material parameter for an orthotropic material, two uniaxial tension tests are required at off-axis angles; typically, three tension tests are done for increased accuracy. Once the material

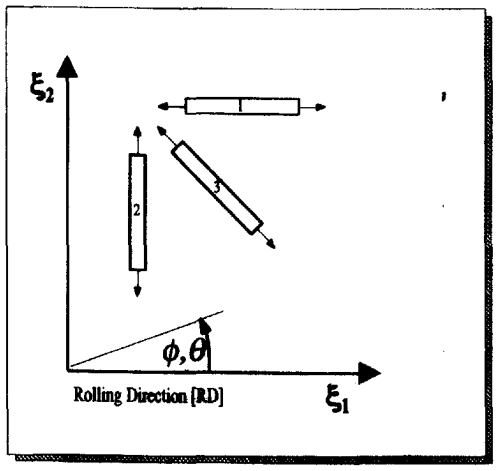

Fig. 4. Uniaxial specimen cut from a rolled plate of aluminum 2024-T351.

parameters are determined, the GAR technique can be applied to structures composed of the same material.

Since the GAR technique is based on the simultaneous measurements of both shear and longitudinal waves, the experiment is conceptually different from similar experiments reported in the literature, which are based on shear or longitudinal waves only (Clark *et al.*, 1983; Dike and Johnson, 1990).

Three calibration specimens were machined from the reference material, a rolled sheet of aluminum 2024-T351, and loaded uniaxially (Fig. 4). Due to the rolling process the material exhibits slight orthotropy and the material symmetry axes are aligned with the rolling, transverse and normal directions of the sheet.

For three different load directions, the absolute time of flight and wave polarization angles are measured as a function of uniaxial tension load. To excite the ultrasonic wave, a 20 MHz piezoelectric transducer was mounted in a holder with a fixed gap of 80 μm and with a viscous fluid providing the acoustic coupling. This set-up allowed reproducible coupling and echoes within the coupling layer were sufficiently delayed so as not to interfere with the outgoing ultrasonic pulse. The transducer also acted as receiver of the back face echoes and transit times were measured with the pulse echo method. At each load step the transit time was measured for both shear waves and the longitudinal wave; the shear wave polarization angles were recorded by rotating the transducer until a maximum echo was received. Further details of the experimental set-up are discussed by Janssen and Zuidema (1985).

Figure 4 shows the orientation of the tension specimens cut from the plate and the coordinate system used for the subsequent analysis; Table 1 lists the dimensions and other relevant information of the specimens. Note that the specimens are not perfectly aligned with the material axes, but are slightly rotated by 1.2°.

To distinguish the two shear waves we denote them as TD (transverse direction) or RD (rolling direction) shear waves. This refers to the alignment of the corresponding polarization vector in the load-free state.

Figure 5 shows the stress dependence on the wave speed for specimen 1 aligned closely with the rolling direction and Fig. 6 shows the associated polarization directions of the shear waves. Note that the shear wave curves appear to be composed of straight segments,

Table 1. Uniaxial tension specimen: dimensions and loading

Thickness:	6.005 mm	Width:	12 mm
Density:	2750 kg m^{-3}	Loading:	0–16 kN
Orientation:	Specimen 1: 1.2°	Specimen 2:	91.2°
	Specimen 3: −43.8°		

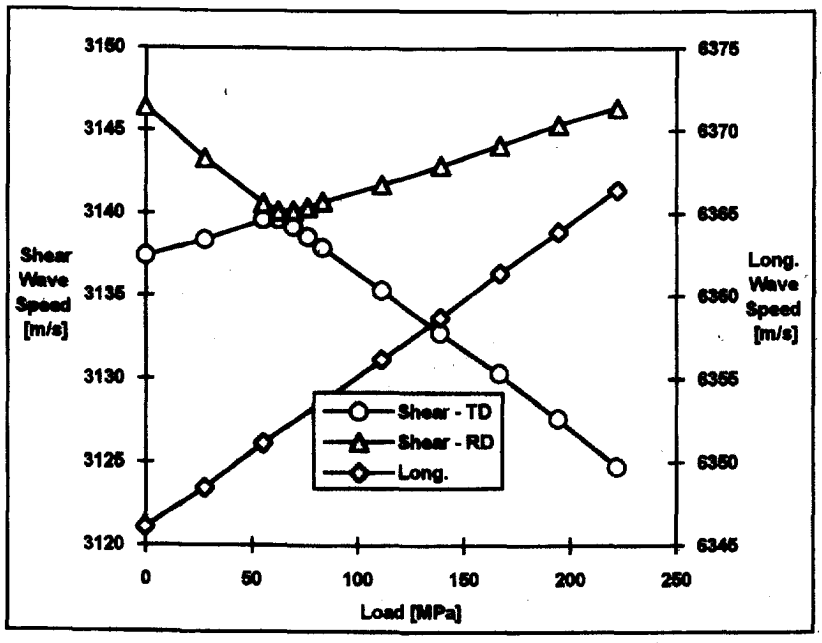

Fig. 5. Uniaxial specimen loaded in the rolling direction : wave speeds.

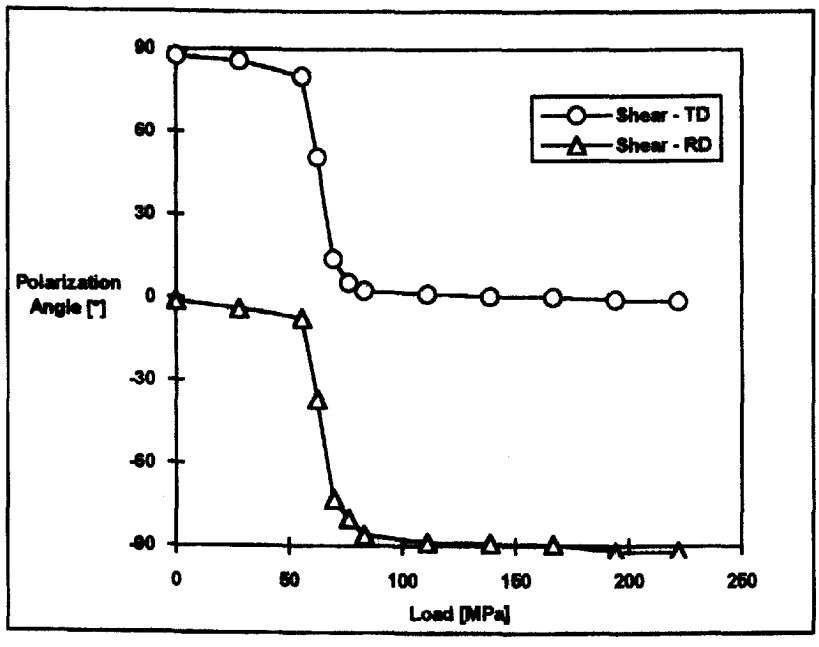

Fig. 6. Uniaxial specimen loaded in the rolling direction : polarization angles.

which almost touch at a load of about 65 MPa. At this load the polarization angles of the shear waves rotate rapidly by 90°. This phenomenon is due to the slight off-axis loading of the specimen and will be explained in detail in the subsequent analysis. The longitudinal wave speed depends linearly on the applied stress.

Specimen 2, which is loaded in the transverse direction, shows a clearly different behavior. Figures 7 and 8 show the measured propagation speed and corresponding polarization angles. Only a linear change in wave speed is observed and the polarization directions remain essentially constant and aligned with the material symmetry axes.

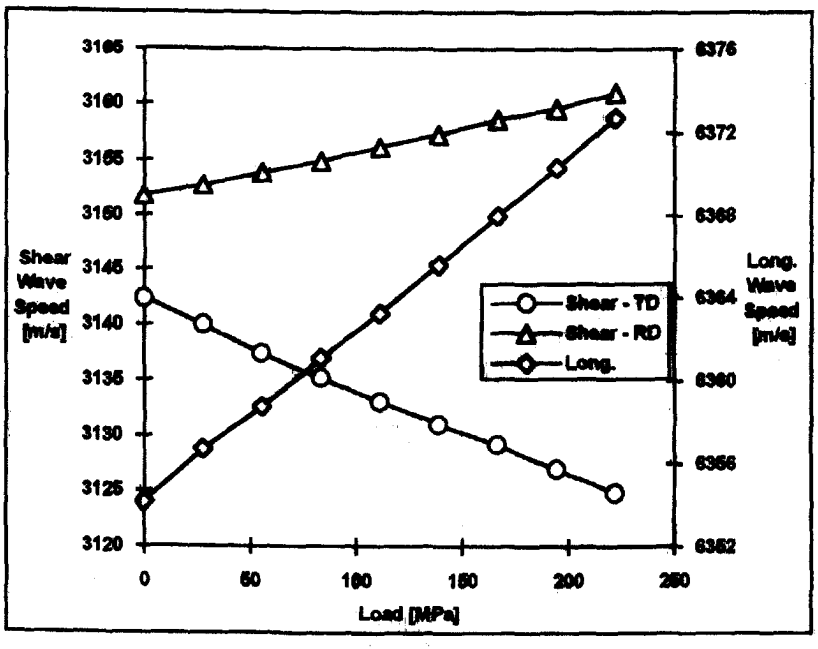

Fig. 7. Uniaxial specimen loaded in the transverse direction: wave speeds.

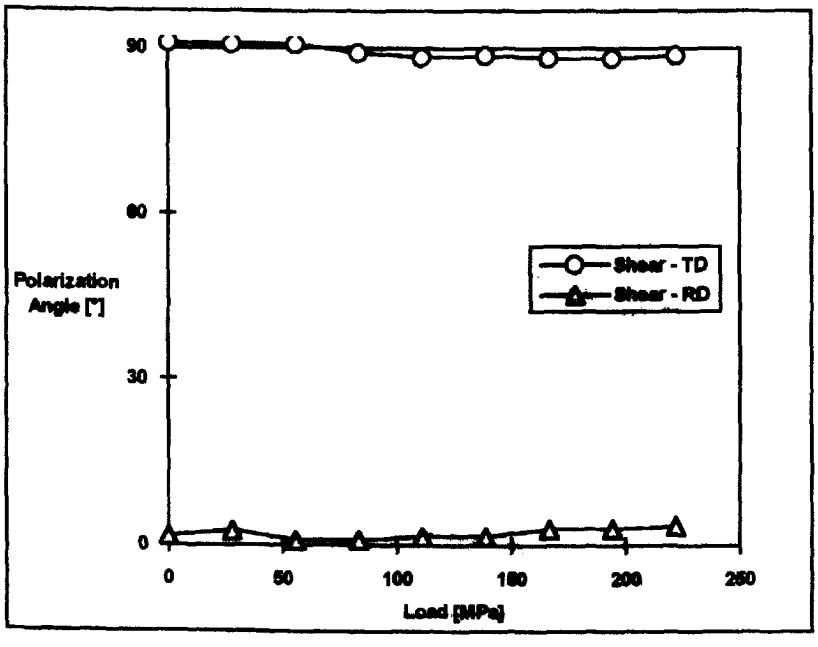

Fig. 8. Uniaxial specimen loaded in the transverse direction: polarization angles.

A nonlinear stress dependence is observed for the shear wave speeds in specimen 3 at an off-axis angle of $-43.8°$. Again, the longitudinal wave speed dependence is linear. The measurements are shown in Figs 9 and 10.

Based on the uniaxial measurements, the unknown material parameters are calibrated from eqns (30), (34) and (41) or directly by reconstruction of the acoustic tensor (21). The measurements at the stress-free state yield the initial birefringence B_0, inverse R-value IR_0, and the elastic stiffnesses C^0_{33}, C^0_{44} and C^0_{55}. The acoustoelastic material parameters h_{ij} are found from the stress dependence. The complete set of calibrated material constants is

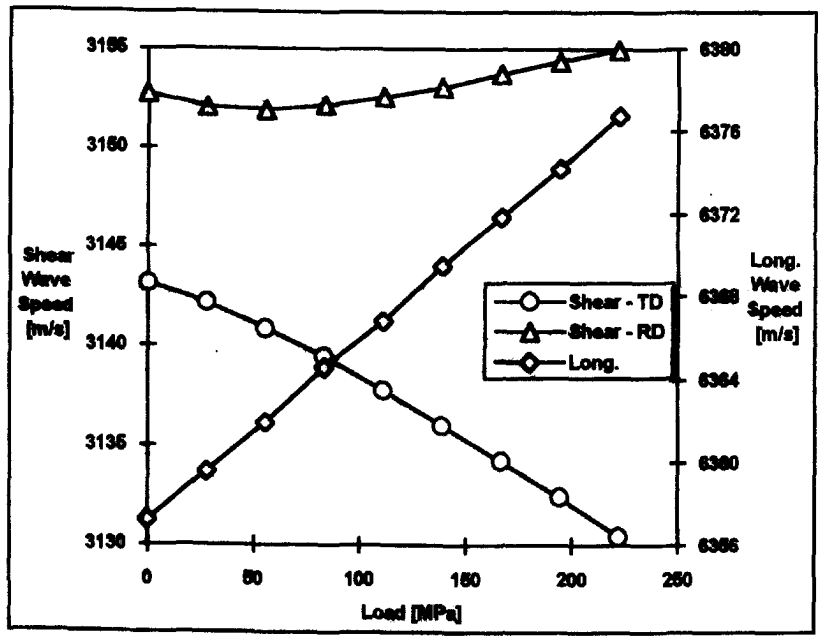

Fig. 9. Off-axis loaded uniaxial specimen: wave speeds.

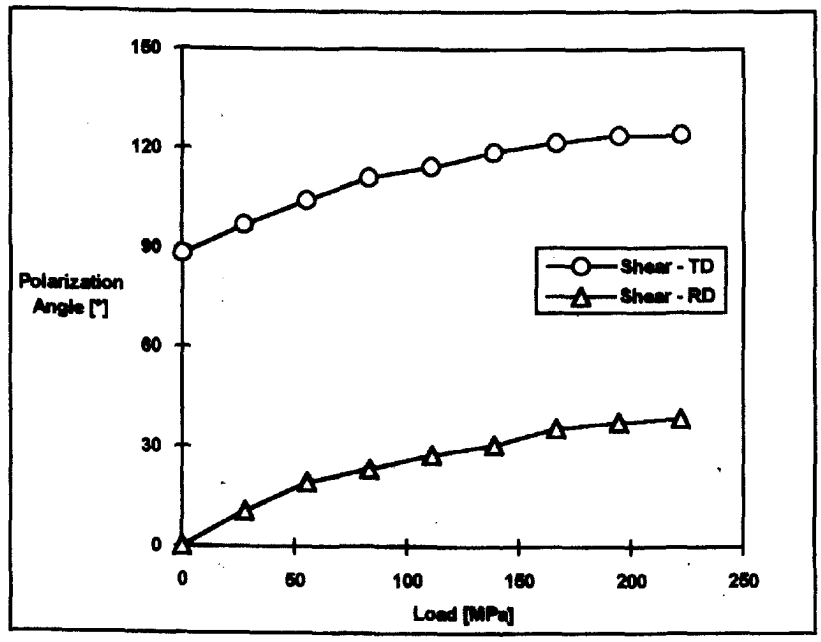

Fig. 10. Off-axis loaded uniaxial specimen: polarization angles.

given in Table 2. These acoustic parameters can now be used to determine the local two-dimensional stress state from measurements performed on a specimen composed of the same material.

It is important to note that the use of a reference sample implies that microstructural differences between the reference and stressed specimen are sufficiently small so that the acoustoelastic constants of both reference and specimen are comparable.

Table 2. Acoustoelastic material parameters

Elastic constants (GPa)	Acoustoelastic constants		
C^0_{55} 27.24	h_{51} −1.651	h_{42} −1.345	h_{45} −1.8414
C^0_{44} 27.08	h_{52} 0.726	h_{31} 3.215	
C^0_{33} 110.8	h_{41} 0.7085	h_{32} 2.9	
Shear birefringence		Inverse R-value	
B_0 0.295%	f_2 −40.8 TPa^{-1}	IR_0 49.5%	
f_1 −2.66 TPa^{-1}	f_3 −33.9 TPa^{-1}	r_A −21.0 TPa^{-1}	
		r_B −2.2 TPa^{-1}	

RESULTS

Based on the identification of the acoustoelastic parameter from the uniaxial tension test, it is now possible to reconstruct the change in wave speed for an arbitrary plane stress state. The nonlinear change of the shear wave speed in slightly orthotropic materials for uniaxial loading is shown in more detail in Fig. 11. The dashed and solid lines refer to shear waves, which are initially polarized in the rolling (RD) and transverse (TD) directions. The nonlinearity disappears for loading parallel to the material symmetry axes.

In Fig. 11 there are two possible stress states, which yield identical shear wave speeds. At these stress states the birefringence is zero and the material is acoustically quasi-isotropic. Equation (47) can be used to determine these loads. For uniaxial stress there are two quasi-isotropic load states: tension loading of 68 MPa in the rolling direction and compression loading of −77 MPa in the transverse direction. Figure 12 shows the polarization angle of the shear waves initially polarized in the rolling direction; the wave rotates under load increase and is rather sensitive to the load angle. Very rapid rotation occurs near the quasi-isotropic loads and load angles. This feature was indeed observed in the experiments, where the small off-axis angle (1.2°) caused a rapid rotation of the polarization angles near the uniaxial loading (68 MPa) of acoustic quasi-isotropy.

Figure 13 shows the dependence of the acoustic birefringence on load angle and uniaxial load as calculated from the calibration constants. The triangular markers denote the directly measured birefringence as calculated from the raw experimental data (time of flight). The data in Fig. 13 are normalized with respect to the initial birefringence

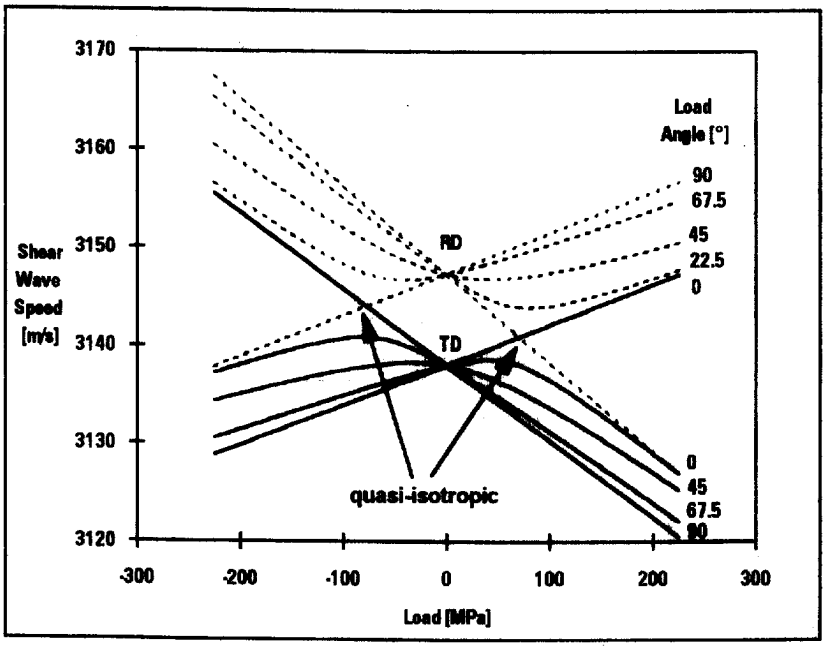

Fig. 11. Shear wave dependence under uniaxial loading.

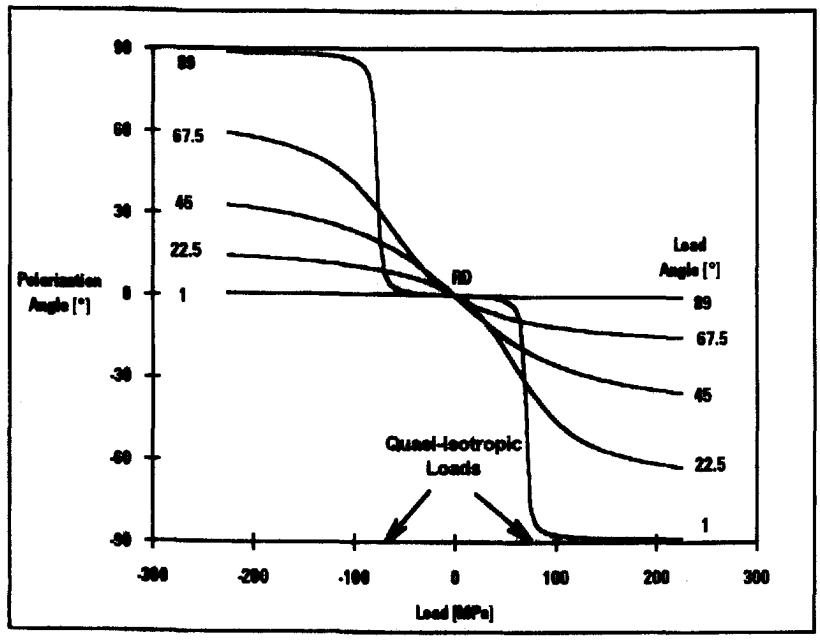

Fig. 12. Shear wave polarization angles under uniaxial loading.

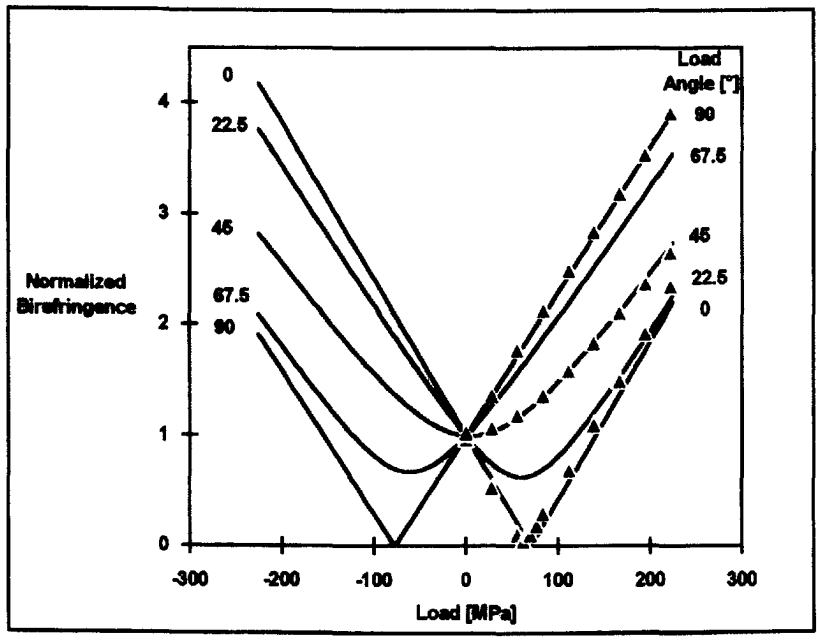

Fig. 13. Shear wave birefringence under uniaxial loading.

(2.946×10^{-3}). It is apparent that the theoretical birefringence predictions agree well with the measurements.

Similar results were also found in a theoretical study of birefringence in slightly anisotropic materials by Iwashimizu and Kubomura (1973). The objective here is to correlate the experimental data with the theoretical predictions based on the GAR technique.

Comparison of the calibrated values f_1, f_2 and f_3 shows that f_1 is an order of magnitude smaller than f_2 and f_3. Therefore, the birefringence (32) depends primarily on the difference in principal stresses, which is characteristic of weakly anisotropic materials.

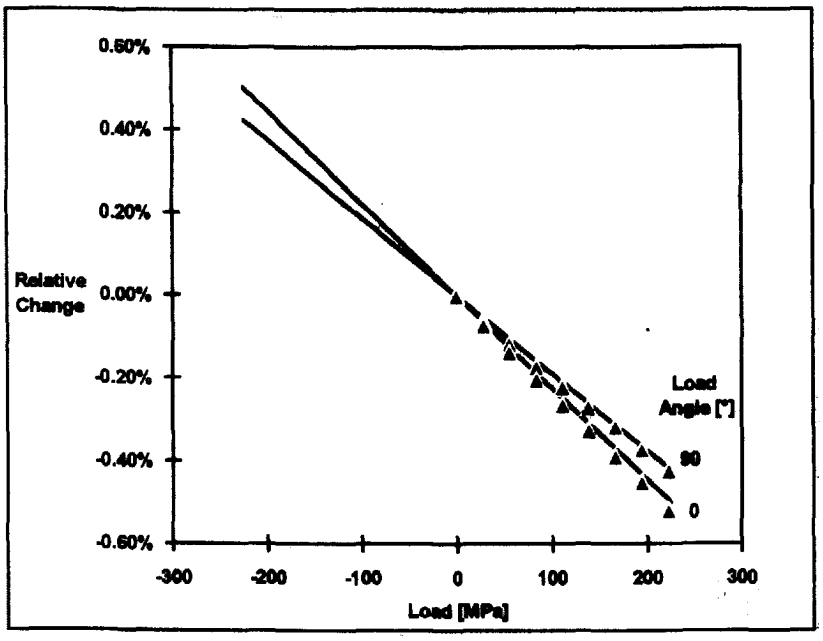

Fig. 14. Inverse R-value under uniaxial loading.

The second acoustic ratio used in the GAR technique is the inverse R-value; its stress dependence for the analysed material is plotted in Fig. 14. The triangular markers again denote the inverse R-value as calculated directly from the ultrasonic time of flight. The normalization factor is the ratio for the load-free case (0.4951). It is apparent that the R-value depends only linearly on the stress as predicted by the theory. Also, it is rather insensitive to the load angle. This is due to the fact that the R-value is primarily dependent on the sum of the principal in-plane stresses in weakly anisotropic materials. For the given material the ratio of the acoustoelastic coefficients r_A/r_B is approximately 10, which is another indicator of the weak anisotropy. The disadvantage of the R-value is its relatively small change, only 0.6% at the yield point of the reference material.

CONCLUSIONS

The GAR technique is a new method for the ultrasonic measurement of two-dimensional stress fields. Based on the transit times of the three ultrasonic wave modes and the shear wave polarization angle, the local in-plane stress can be predicted. Experiments on uniaxial specimens yield the acoustoelastic material parameters and show that the theory accurately predicts the observed phenomena.

Further research is underway to apply the results from uniaxial specimens to the reconstruction of the two-dimensional stress field in compact tension specimens.

Acknowledgement—This work was partially supported by a grant from the Gleason Memorial Fund.

REFERENCES

Benson, R. W. and Raelson, V. J. (1959). Acoustoelasticity. *Product Engng* **30**, 56–59.

Bergman, R. H. and Shahbender, R. A. (1958). Effect of statically applied stresses on the velocity of propagation of ultrasonic waves. *J. Appl. Phys.* **29**, 1736–1738.

Clark, A. V., Mignogna, R. B. and Stanford, R. J. (1983). Acoustoelastic measurement of stress and stress intensity factors around crack tips. *Ultrasonics* **21**, 217.

Crecraft, D. I. (1967). The measurement of applied and residual stresses in metals using ultrasonic waves. *J. Sound Vibr.* **5**, 173–192.

Dike, J. J. and Johnson, G. C. (1990). Residual stress determination using acoustoelasticity. *Trans. ASME* **57**, 12–17.

Dorfi, H. (1994). Acoustoelasticity: stress identification based on ultrasonic measurements. Dissertation, Department of Mechanical Engineering, The Ohio State University, Columbus, OH.

Hearmon, R. F. S. (1953). Third order elastic coefficients. *Acta Crystallogr.* **6,** 331–340.

Hughes, D. S. and Kelly, J. L. (1953). Second-order deformation of solids. *Phys. Rev.* **92,** 1145–1149.

Iwashimizu, Y. and Kubomura, K. (1973). Stress-induced rotation of polarization directions of elastic waves in slightly anisotropic materials. *Int. J. Solids Structures* **9,** 99–114.

Janssen, M. and Zuidema, J. (1985). An acoustoelastic determination of the stress tensor in textured metal sheets using the birefrigency of ultrasonic shear waves. *J. Nondestruct. Eval.* **5,** 45–52.

Johnson, G. C. (1981). Acoustoelastic theory for elastic–plastic materials. *J. Acoust. Soc. Am.* **70,** 591–595.

Kobayashi, M. (1990). Acoustoelastic theory for plastically deformed solids. *JSME Int. J. Ser.* 1 **33,** 310–318.

Pao, Y.-H., Wu, T.-T. and Gamer, U. (1991). Acoustoelastic birefringes in plastically deformed solids: Part I—Theory. *J. Appl. Mech.* **58,** 11–17.

Pao, Y.-H., Sachse, W. and Fukuoka, H. (1984). Acoustoelasticity and ultrasonic measurements of residual stresses. *Phys. Acoust.* **XVII,** 61–143.

Thurston, R. N. and Brugger, K. (1964). Third-order elastic constants and the velocity of small amplitude elastic waves in homogeneously stressed media. *Phys. Rev.* **133,** 1604–1612.

Toda, H., Fukuoka, H. and Aoki, Y. (1984). *R*-value acoustoelastic analysis of residual stress in a seam-welded plate. *Jap. J. Appl. Phys. Suppl.* **23,** 86–88.

Toupin, R.A. and Bernstein, B. (1961). Sound waves in deformed perfectly elastic materials. Acoustoelastic effect. *J. Acoust. Soc. Am.* **33,** 216.